Eur. Phys. J. B **65**, 353–359 (2008)
DOI: 10.1140/epjb/e2008-00291-9

THE EUROPEAN PHYSICAL JOURNAL B

Infection fronts in contact disease spread

U. Naether[1], E.B. Postnikov[2], and I.M. Sokolov[1,a]

[1] Institut für Physik, Humboldt-Universität zu Berlin, Newtonstr. 15, 12489 Berlin, Germany
[2] Department of Theoretical Physics, Kursk State University, 305000, Radishcheva 33, Kursk, Russia

Received 8 January 2008 / Received in final form 22 May 2008
Published online 18 July 2008 – © EDP Sciences, Società Italiana di Fisica, Springer-Verlag 2008

Abstract. We analyze the epidemic spread via a contact infection process in an immobile population within the Susceptible-Infected-Removed (SIR) model. We present both the results of stochastic simulations assuming different numbers of individuals (degrees of freedom) per cell as well as the solution of the corresponding deterministic equations. For the last ones we show that the appropriate system of nonlinear partial differential equations (PDE) allows for a complete separation of variables and present the approximate analytical expressions for the infection wave in different ranges of parameters. Comparing these results with the direct Monte-Carlo simulations we discuss the domain of applicability of the PDE models and their restrictions.

PACS. 87.23.Cc Population dynamics and ecological pattern formation – 87.10.Ed Ordinary differential equations (ODE), partial differential equations (PDE), integrodifferential models – 87.10.Mn Stochastic modeling

1 Introduction

In a century after the first publication on mathematical theory of epidemics by Ross a lot of work has been done devoted to the description of disease spread in a population, see [1] for a comprehensive review. One of the simplest, useful and popular models is the SIR scheme. It describes a population consisting of three kinds of individuals, namely the susceptible (S), the infected (I), and the recovered/removed (R) ones. The transitions between these states are governed by the infection transmission rate κ and the characteristic recovery time τ:

$$S \stackrel{\kappa}{\rightarrow} I \stackrel{1/\tau}{\rightarrow} R.$$

There exist various implementations of this scheme which correspond to different assumptions about the spatial structure of population and its mixing dynamics. For example, the the Kermack-McKendrick model (KMcK) [2]

$$\frac{dS}{dt} = -\kappa SI, \tag{1}$$

$$\frac{dI}{dt} = \kappa SI - \frac{1}{\tau}I, \tag{2}$$

$$\frac{dR}{dt} = \frac{1}{\tau}I, \tag{3}$$

assumes perfect mixing, which completely eliminates a spacial aspect of behavior. To take mobility into account, the Fisher-Kolmogorov-Petrovsky-Piskounov (FKPP)-like models [3,4] add diffusion terms to the right-hand-sides of equations (1–3). Kendall [6] proposed a different approach, namely, using a spatially averaged concentration of infected $\langle I(x)\rangle$ around the spatial point considered instead of the local $I(x)$ in the reaction terms of equations (1–3). The Taylor expansion of this average up to the second term leads then to the following system of equations:

$$\frac{\partial S}{\partial t} = -\kappa SI - DS\frac{\partial^2 I}{\partial x^2}, \tag{4}$$

$$\frac{\partial I}{\partial t} = \kappa SI + DS\frac{\partial^2 I}{\partial x^2} - \frac{1}{\tau}I, \tag{5}$$

$$\frac{\partial R}{\partial t} = \frac{1}{\tau}I \tag{6}$$

(where we confine ourselves to a one-dimensional notation), with D/κ denoting the second Taylor's coefficient, provided that the first one vanishes. For the review of this and similar approaches see also the references [7,8]. Under the corresponding choice of parameters the variables S, I and R can be interpreted as the probabilities for an individual to be susceptible, infected or recovered, which means that since the sum $S + I + R$ is conserved, this sum can be put to unity. The probability for a cell to be infected can only change in case the cell is susceptible and depends on the number of its infected nearest-neighbors. One of the particular realizations of this model was considered in [9] discussing disease propagation through a population of individuals which are either immobile or show a high degree of site fidelity.

[a] e-mail: igor.sokolov@physik.hu-berlin.de

The main goal of the present paper is a further analysis of the deterministic equations (4–6) as well as the Monte-Carlo simulations of the corresponding stochastic model taking into consideration other aspects of the propagation process. This one is a generalization of the models of references [10,11], related to percolation, in which we now allow for more than one individual per site. The comparison of predictions of the deterministic model with the results of the simulations of the stochastic one allows to discuss the details of transition from the microscopic to the macroscopic level of description and to determine the area of applicability of the deterministic approach.

2 Monte-Carlo simulations

Let us first turn to simulations of infection spread through the population distributed over the patches (cells), which include various numbers of individuals. It is a natural step to determine an appropriate level of coarse-graining which admits the continuous description via PDE system.

2.1 Model

We consider the SIR-system on a 2D square lattice of $N_x \times N_y$ sites with the lattice spacing a and cyclic boundary conditions. For simplicity, the columns and the rows of the lattice are marked by x and y considered at the beginning as whole numbers. It is admitted that each cell includes a variable number r of individuals, i.e. internal degrees of freedom. The transmission of infection through the whole system is only due to interaction between individuals from next-neighbor cells. This leads to the refinement of a disease grade with the growth of the number r of internal degrees of freedom (individuals per cell). The possibility of infection transmission within the cell is disregarded in our simulations, which makes it unnecessary to renormalize the infection rate κ with the number of the degrees of freedom. In this case the number r corresponds simply to the degree of coarse graining of the description. The possibility of infection within one cell only leads to the effective renormalization of parameters of the corresponding model.

Quantitatively, the probability of infection p_I for a susceptible summed over all orientations is

$$p_I = \Delta t \left(1 - (1 - \kappa/4)^{\sum I_{NN}}\right), \tag{7}$$

where $\kappa/4$ is a probability of infection transmission from the next-neighbor cell during the time interval Δt and

$$\sum I_{NN} = I(x+a,y) + I(x-a,y) + I(x,y+a) + I(x,y-a).$$

The probability p_R for an infected to be removed during Δt is

$$p_R = \frac{1}{\tau}\Delta t \tag{8}$$

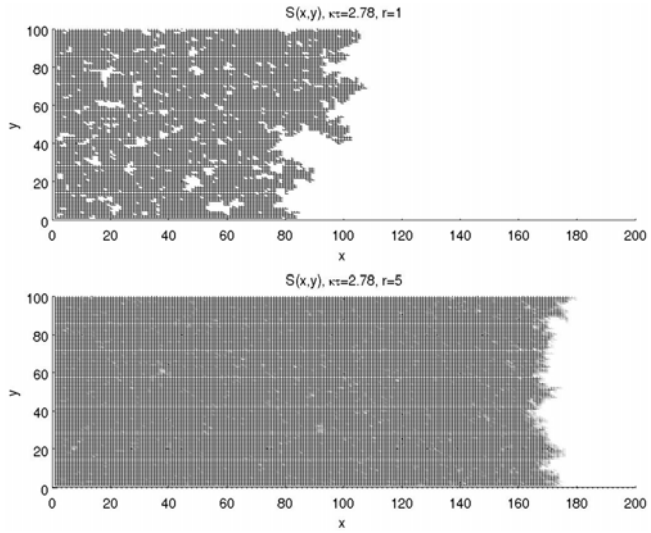

Fig. 1. $S(x,y)$ for $r = 1$ (upper panel) and for $r = 5$ (lower panel) for $t = 500$. The degree of infection in a cell us shown on the grayscale: black $S = 0$, white $S = 1$.

and the normalization condition $I(x,y) + R(x,y) + S(x,y) = 1$ is applied. The time step Δt is chosen small enough ($\Delta t/\tau = 0.005$, where τ is again the characteristic recovery time).

Initially, at $t = 0$, the completely infected ($I(0,y) = 1$) cells are distributed along the first column of the lattice. All other cells are susceptible $S(x,y) = 1$ for all $x \neq 0$. Cyclic boundary conditions are adopted. After several preliminary (parallel) updates, we get a stable propagating front of infection. Its motion is described by the projection on the x-axis via the column average

$$I(x_i(t)) = \frac{1}{N_y}\sum_{i=1}^{N_y} I'(x_i, y_i, t). \tag{9}$$

To determine the front's velocity we look at the position of its center of mass

$$\langle x(t)\rangle = \frac{\sum_i I(x_i(t))x_i(t)}{\sum_i I(x_i(t))}$$

and define the velocity as

$$v_{cm} = \frac{\Delta\langle x(t)\rangle}{\Delta t}.$$

Figure 1 shows the snapshots of the propagating infection front for two different values of r.

2.2 Simulations in 1D

Since our further analysis is mostly pertinent to a one-dimensional case, we start here from presenting the situations for the one-dimensional lattice. To consider a limiting transition to the case of very large number of internal degrees of freedom (i.e. individuals per cell), we simulate the spread over 1000×1 lattice. Figure 2 represents

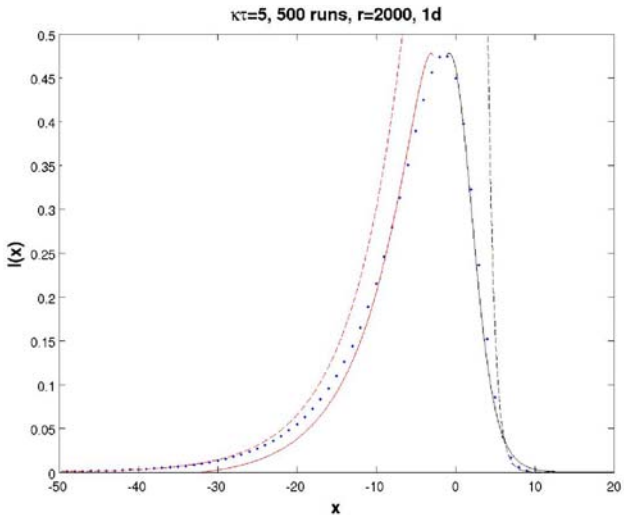

Fig. 2. The shape of the infection wave in 1D together with some analytical approximations for $\kappa\tau = 5$ and $r = 2000$. The dots are the results of simulations as averaged over 500 runs. The dashed lines are the exponential leading edge and far tail approximations, while the dotted and the solid lines give the non-exponential analytical approximations for the front and wake of the infection wave, see Section 3.

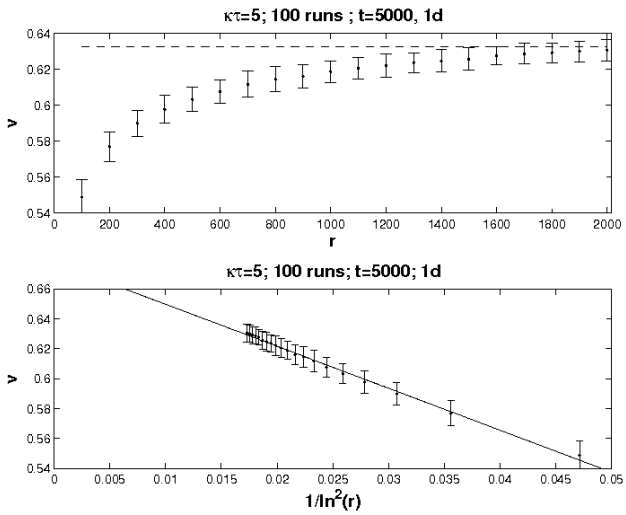

Fig. 3. Mean velocity as the function of the number of states per cell. Upper panel: linear scales; lower panel: v_r as a function of $1/\ln^2(r)$. The dashed line in the upper panel denotes the limiting velocity $v_{min} = 2\sqrt{D(\kappa - \tau^{-1})}$.

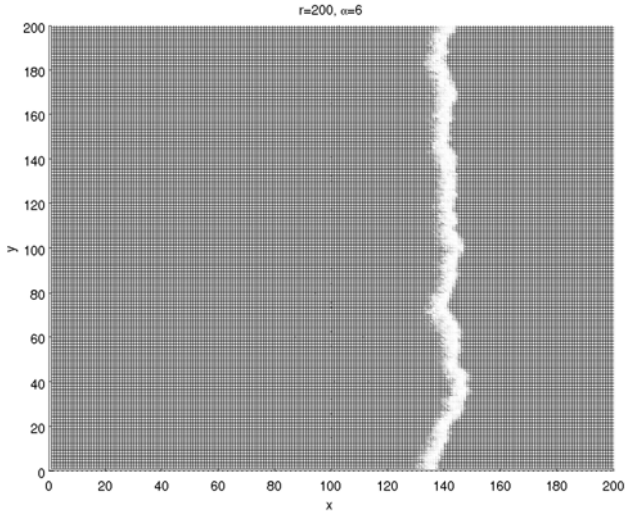

Fig. 4. The infection wave for $\kappa\tau = 6$ and $r = 200$. Shown is the concentration of infected on the grayscale.

the form of the spreading wave for the simulation with $r = 2000$ (dots) and $\kappa\tau = 5$ and its comparison with different analytical results. The full-range approximations of front and tail from Sections 3.2 and 3.3 are shown with solid lines, and the exponential behavior in far tail region and in the leading edge [9] are shown with dashed lines. One readily infers that the analytical approximations based on the solution of the PDEs give a very good description of the overall form of the wave as both its shape and its maximum height are concerned. The leading edge and the far tail behavior are adequately captured by exponential asymptotics. The corresponding calculations are based on the front propagation velocity as given by the marginal stability principle, which proves that the overall continuous description in 1D is valid for such a large number of individuals per cell.

Now let us consider the dependence of the infection wave's properties on this number and first concentrate on the velocity of the wave as a function of the number of individuals per cell. In this case the discreteness of the system plays a role and the propagation velocity is typically slower than the one given by the continuous treatment (see e.g. [12–14]). This behavior can be also seen in the stochastic FKPP equation [15]. In the 1D case, Brunet and Derrida [16] introduced a cutoff of the local concentration $h \geq 1/r$ for the FKPP-type equations and found the lowest order correction v_r to the velocity v_0:

$$v_r \simeq v_0 - \frac{b}{(\ln r)^2} \quad \text{for} \quad 1/\ln r \ll 1 \tag{10}$$

with some constant b. The lower panel of Figure 3 clearly shows this overall kind of behavior, however, the extrapolation of the corresponding straight line to $r \to \infty$ gives as a result the value of asymptotic velocity somewhat higher than the one given by the continuous approximation. The reason can be the finite simulation time, but still has to be analyzed in detail.

2.3 Wave's shape in 2D

In Figure 4 the spread of the infection wave is plotted for $\kappa\tau = 6$ and $r = 200$ – the front of the wave is quite rough, and one has to decide how to take this roughness into account and how to eliminate its effect on the results for the velocity and for the form of the front.

The simplest possibility is the projection of the whole wave's profile onto the x-axis (9) and then an averaging over K runs of the simulation with a "cut and shift" of

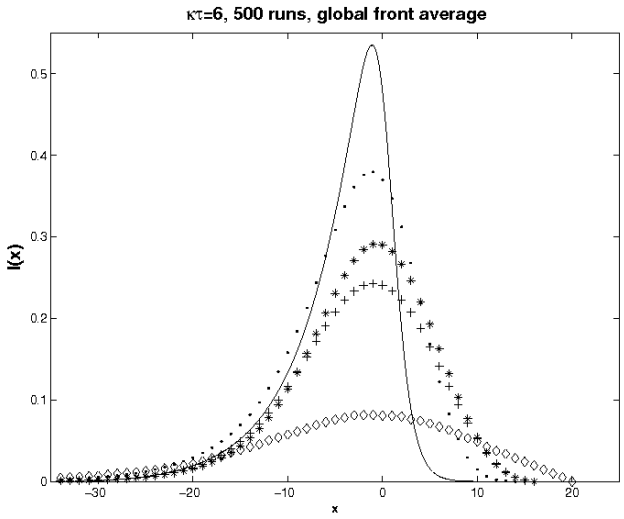

Fig. 5. The shape of the infection wave for different numbers of states per cell under global averaging, $\kappa\tau = 6$. The symbols correspond to the simulations with $r = 1$ (diamonds), $r = 5$ (crosses), $r = 10$ (asterisks) and $r = 200$ (dots). The solid line represents the analytical result from the PDE solution.

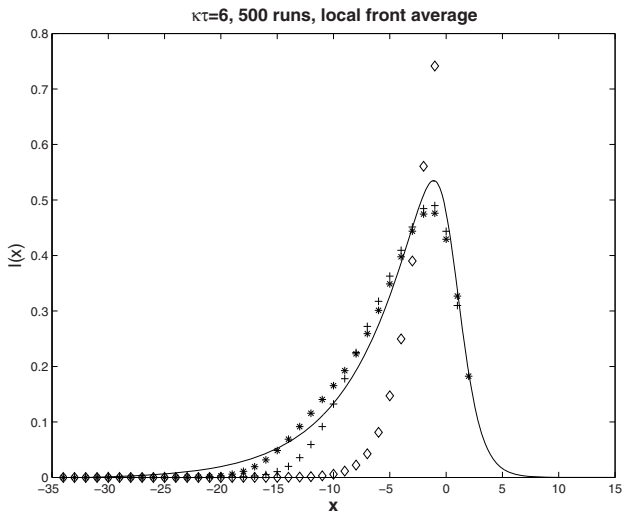

Fig. 6. The shape of the infection wave for different numbers of states per cell under local averaging, $\kappa\tau = 6$ for $r = 1$ (diamonds), $r = 5$ (crosses) and $r = 10$ (asterisks). The full line is the PDE solution.

the infected at every run k in such a way that the position of the rightmost infected in each run coincide:

$$\langle I(x_f - x_i)\rangle_K = \frac{1}{K}\sum_{k=1}^{K} I(x_{f,k} - x_i). \tag{11}$$

The "cut and shift" prescription is necessary to avoid influence of velocity fluctuations. Here $x_{f,k}$ is the position of the foremost infected in the k-th run, which is shifted to a fixed x_f, and x_i are all following lattice points. This procedure will be referred to as a global averaging. The cutting and shifting at every row y according to equation (11) first and then projecting onto the x-axis and averaging over runs afterwards will be called local averaging.

In Figure 5 the global averaged infection wave for $\kappa\tau = 6$ on a 400×600 lattice and $r = \{1, 5, 10, 200\}$ is shown. The difference between the simulated wave forms under global averaging and the results of the analytical approaches of Sections 3.2 and 3.3, plotted with solid curves, is evident for all r both in the front form of the wave and in the lower value of its maximum. The difference between discrete and continuous description gets smaller with the growth of the number of internal degrees of freedom (individuals per cell). This difference is caused by the kinetic roughening [17] and gets much milder if the local averaging procedure is applied.

If the results of the very same simulations are proceeded according to the local averaging procedure, the shape looks like the one in Figure 6 for $r = \{1, 5, 10\}$ and as the one in Figure 7 for ($r = 200$). Solid lines represent the analytical approaches of Sections 3.2 and 3.3 and the excellent agreement for higher state numbers per point is shown. The mismatch for smaller r is easy to understand since the continuous approximation is only assumed to work well for $I(x) \gg \frac{1}{r}$.

As a summary, we point out that kinetic roughening leads to an broadening of the front of an epidemic wave, but under local averaging the 1D continuous description is still valid. Furthermore, the growth of the number of individuals inside a cell leads to the convergence of the discrete simulation results and the continuous functions given by PDE system both for the wave's shape and for its velocity.

3 Analysis of PDE system and its approximate solution

3.1 Infection wave in a comoving frame: separation of variables

Let us now turn to the continuous description and consider a stationary infection wave propagation. Changing to a comoving frame $x' = x - vt$, where v is the infection wave's propagation velocity, we get:

$$-v\frac{dS}{dx'} = -\kappa SI - DS\frac{d^2I}{dx'^2}, \tag{12}$$

$$-v\frac{dI}{dx'} = \kappa SI + DS\frac{d^2I}{dx'^2} - \frac{1}{\tau}I, \tag{13}$$

$$-v\frac{dR}{dx'} = \frac{1}{\tau}I. \tag{14}$$

Let us show that the system of equations (12–14) allows for a complete separation of variables. Using the fact that $S+I+R = 1$ everywhere, one can rewrite equation (12) as

$$-v\frac{dS}{dx'} = -\kappa S(1 - S - R) - DS\frac{d^2}{dx'^2}(1 - S - R).$$

Regrouping the variables, we get

$$v\frac{dS}{dx'} = \kappa S(1 - S) - DS\frac{d^2S}{dx'^2} - S\left(\kappa R + D\frac{d^2R}{dx'^2}\right). \tag{15}$$

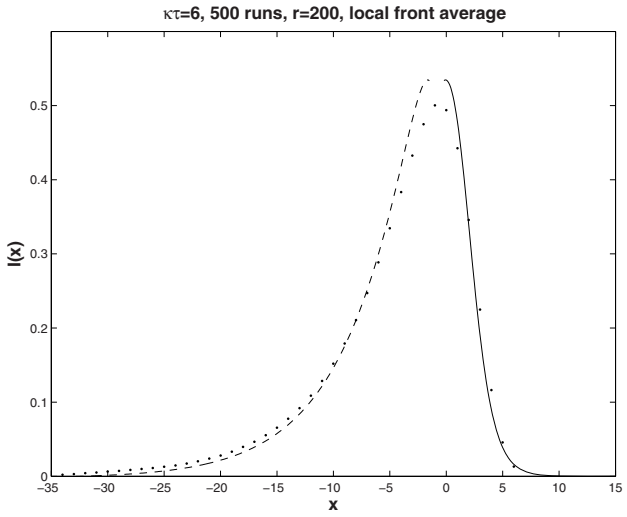

Fig. 7. Same as in Figure 6, now for $r = 200$. The dashed and the full lines represent the analytical approximations for the wake and for the front of the wave.

Let us now return to equation (12), divide its both sides by S, getting

$$v\frac{d\ln S}{dx'} = \kappa I + D\frac{d^2 I}{dx'^2} \tag{16}$$

and substitute I in the right-hand-side of this equation by dR/dx' according to equation (14):

$$v\frac{d\ln S}{dx'} = -\kappa\tau v\frac{dR}{dx'} - D\tau v\frac{d}{dx'}\frac{d^2 R}{dx'^2}.$$

This last equation can be rewritten in a form

$$\frac{d}{dx'}\left(\ln S + \kappa\tau R + D\tau\frac{d^2 R}{dx'^2}\right) = 0.$$

This means that our initial system of equations possesses an integral of motion

$$\ln S + \kappa\tau R + D\tau\frac{d^2 R}{dx'^2} = C_0 = \text{const}.$$

We note here that such an integral of motion exists also for the initial system of equations (4–6), as it was pointed out by Grassberger [10]. To determine the value of the constant C_0, consider the region $x \to \infty$, far in front of the infection wave. In this domain $S = 1$ (and $\ln S = 0$) and $R = \frac{d^2 R}{dx'^2} = 0$. Consequently, $C_0 = 0$, so that

$$\ln S + \kappa\tau R + D\tau\frac{d^2 R}{dx'^2} = 0. \tag{17}$$

Now we can insert equation(17) into equation (15). As a result, a closed equation for S emerges:

$$v\frac{dS}{dx'} = \kappa S(1-S) - DS\frac{d^2 S}{dx'^2} + \frac{1}{\tau}S\ln S. \tag{18}$$

If the solution of equation (18) is known, equation (17) allows for finding R, after which the solution for I follows from equation (14) or by using the fact that $S+I+R = 1$.

The corresponding equations for R and for I are related to the equation of motion of a harmonic oscillator under an external forcing:

$$\frac{d^2 y}{dx'^2} + \omega^2 y = F(x'). \tag{19}$$

Here y is R or I, $\omega = \sqrt{\kappa/D}$, and the external force is $F(x') = -(D\tau)^{-1}\ln S(x')$ for $y = R$, and $F(x') = \frac{v}{D}\frac{d}{dx'}(\ln S(x'))$ for $y = I$. The solution of this equation can be obtained using the Fourier representation and reads:

$$y(x') = \text{Im}\left[\frac{\mathrm{e}^{i\omega x'}}{i\omega}\left(\int_{-\infty}^{x'} F(x')e^{-i\omega x'}dx' + y_0(x')\right)\right],$$

where $y_0(x')$ is a solution of the corresponding homogeneous equation, i.e. of equation (19) with $F = 0$.

3.2 Approximate solution: leading front

The leading edge of the front corresponds to the asymptotic exponential solution for very small I and has been analyzed in [9], see also Section 2.3. Thus, we turn to the main part of the front of the reaction wave, the one close to the inflection point. In this part of the front the second derivative in (18) is small and can be neglected. As we proceed to show this is a reasonable approximation describing quite well the largest part of the front up to the maximum of the infection wave. Since S is still close to unity in the front of the infection wave, one can use the Taylor expansion and put $\ln S = \ln(1-(1-S)) \simeq -(1-S)$. Then equation (18) takes the form

$$v\frac{dS}{dx'} = (\kappa - \tau^{-1})\ S(1-S).$$

Taking the velocity to be $v = v_{min} = 2\sqrt{D(\kappa - \tau^{-1})}$, as following from the marginal stability principle, we get the approximate equation for the part of the leading front close to the inflection point in a form

$$\frac{dS}{dx'} = \frac{v}{4D}S(1-S). \tag{20}$$

The solution to equation (20) reads:

$$S(x') = \frac{1}{2}\left[1 + \tanh\left(\frac{v}{8D}(x' - x'_0)\right)\right], \tag{21}$$

where x'_0 is an appropriate shift given by initial conditions.

To determine the shape of the infection leading front for I, we use the conservation law $I = 1 - S - R$ and the integral of motion equation (17) for the determination of R. Neglecting the term with the second derivative again, we get a simple result for this region:

$$I(x') = 1 - S(x') + \frac{1}{\kappa\tau}\ln S(x'), \tag{22}$$

where $S(x')$ is the solution of equation (21).

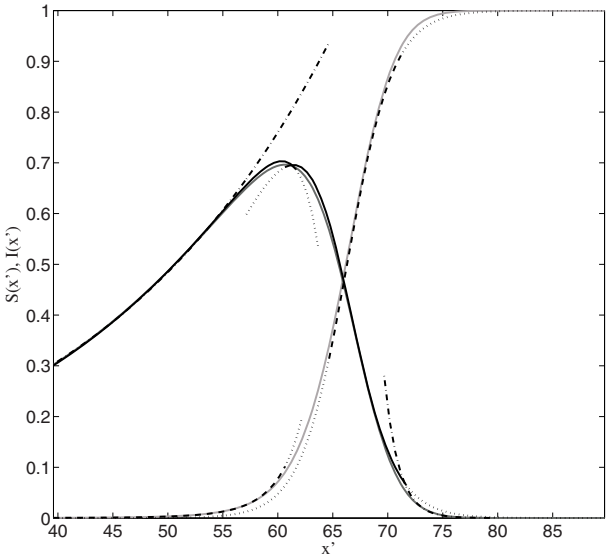

Fig. 8. The comparison of the numerical and analytical approximate solutions for the supercritical case, see the explanation in the text.

Let us consider two numerical examples. The parameters of the first one are taken from reference [9] and correspond to the overcritical case leading to a strongly asymmetrical Kendall wave: we namely take $D = \kappa = 0.75$, $\tau = 15$. Figure 8 represents the full numerical solutions for S (light gray line) and for I (dark gray line) as well as the approximations. The dash-dotted curves are the asymptotic exponential solutions for I from [9]. It is clear that this approximation is valid only far in the leading edge of the front. In the main front's part one readily infers that the approximate solution equation (22) practically coincides with the numerical one over a sufficiently large region of the front (black curve), from the domain where the exponential asymptotics looses its accuracy up to the point of maximum; the behavior of the approximations outside this domain are shown with dotted lines. The approximation equation (21) shown with dashed black line in the region where the approximation performs well (and with the dotted line elsewhere) reproduces the numerical solution for S (light-grey line) very well over the whole region. Moreover, the transition area from $S \simeq 1$ to the $S \simeq 0$ is close to the straight line, which confirms the assumption that the second derivative is small.

Another example corresponds to a case close to criticality: we still take $D = \kappa = 0.75$ but choose $\tau = 3$. Figure 9 shows, that the approximation is still quite adequate over the whole front region up to the point of maximum. The coincidence of the exact numerical (dark gray line) and approximate (black lines) solutions is however somewhat worse than in the supercritical case.

3.3 Approximate solutions in the wake of the infection wave

Let us consider now the wake (rear tail) of the infection wave. At difference with the description of the leading front, the critical and supercritical conditions need various approximations, which fact is connected to the strongly different densities of susceptible population behind the wave in these cases. Namely, in the case of short recovery time which is characteristic for the situation close to criticality, the region behind the front contains relatively large amount of the individuals which have never been infected. This is mirrored by the flat non-zero tail in Figure 9 (light gray line).

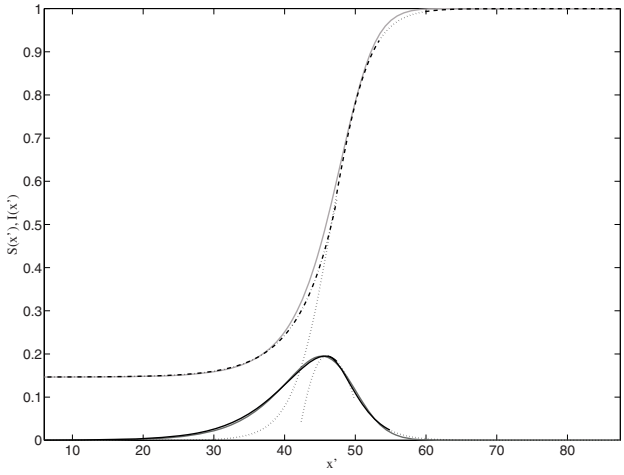

Fig. 9. The comparison of the numerical and analytical approximate solutions for the near-critical case, see the explanation in the text.

The density of never infected population can be found as follows: consider the invariant equation (17). Far in the tail of the wave the density of infected vanishes, and the densities of removed and of susceptible reach their limiting values: $I = 0$, $R = R_- = \text{const}$, and $R_- + S_- = 1$. Therefore, the invariant equation (17) takes the form

$$\ln S_- + \kappa\tau(1 - S_-) = 0 \quad \text{or} \quad S_- = e^{\kappa\tau(S_- - 1)}. \tag{23}$$

This transcendental equation has the solution

$$S_- = -\frac{W(-S_0\kappa\tau \exp(-\kappa\tau))}{\kappa\tau} \tag{24}$$

where $W(z)$ is the so-called Lambert-function, the solution of $z = We^W$.

The exponential asymptotics for this case can be easily derived by taking $S(x') = S_- + s(x)$ (with $s(x) \ll S_-$) in (18) and subsequent linearization of the equation for $s(x')$. Using the expansion $\ln S = \ln(S_-(1 + s/S_-)) = \ln S_- + s/S_-$ and the first form of equation (23) we get the linearized equation

$$DS_- \frac{d^2 s}{dx'^2} + v\frac{ds}{dx'} + \left(\kappa S_- - \frac{1}{\tau}\right) s = 0. \tag{25}$$

As usual, the exponential substitution $s(x') = \exp(\gamma x')$ leads to the characteristic equation

$$DS_-\gamma^2 + v\gamma + \kappa S_- - \frac{1}{\tau} = 0,$$

which has the roots

$$\gamma = -\frac{v}{2DS_-} \pm \sqrt{\left(\frac{v}{2DS_-}\right)^2 - \frac{\kappa S_- - 1/\tau}{DS_-}}. \qquad (26)$$

Only the positive solution has a physical meaning, since S is increasing function of x'. The full function $S = S_- + C_S \exp(\gamma x')$, where C_S is an appropriate constant, is drown in Figure 9 as the black curve. As above, the dependence for $I(x')$ is given by equation (22). The corresponding curve is represented in Figure 9 as the black one. This solution approximates the numerical one (dark grey curve) quite satisfactory up to the maximum of the infection wave where it meets the front approximation considered in Section 3.2.

In the supercritical case the approach considered above is no more applicable since the fast growing $s(x)$ gets large compared to S_-. However, here S itself is quite small so one can neglect both the quadratic term and the second derivative in (18) and gets

$$\frac{dS}{dx'} = \frac{\kappa}{v} S + \frac{1}{v\tau} S \ln S.$$

Dividing both sides of this equation by S gives us a linear equation for $\ln S$:

$$\frac{d}{dx'} \ln S = \frac{\kappa}{v} + \frac{1}{v\tau} \ln S. \qquad (27)$$

Taking an exponential of the solution of equation (27), we get the approximation for the function S for large negative x':

$$S(x') = \exp\left(C \exp\left(\frac{x'}{v\tau}\right) - k\tau\right), \qquad (28)$$

where C is a constant. The solution for the tail of the infection wave is obtained by substitution of (28) into (22). The results for S and for I are given in Figure 8 and show the good performance of the approximation in the whole wake region of the infection wave.

4 Summary

We have considered the spread of a contact infection following the SIR scheme through an immobile population. Both deterministic macroscopic (PDE) and stochastic microscopic (Monte-Carlo) approaches are applied.

It is shown, that the continuous description is not valid for small numbers of cell's states. The results of Monte-Carlo simulations also reveal the conditions of applicability of the PDE approach, which works if elementary "points" of continuous field equations correspond to cells having a large enough number of internal states (considerable local population density). Note, that the quite satisfactory description of the infection spread among the harbor seals in [9] was based on the consideration of animal's groups with strong mixing within a population located in one site and the infection transmission between sites only via contacts between individuals performing rare relatively long trips, so the data was fitted for real-life examples.

Last but not least, it should be pointed out that the corresponding partial differential equations allow not only asymptotic but full-range approximate analytical consideration. The obtained closed-form approximations fit the numerical solution for the critical as well as supercritical cases. This fact opens the opportunity for the continuous analysis of more complicated situations like an epidemic spread through multi-species metapopulations. Recently, this class of equations was successfully applied to the mean-field description of growth of kinetic aggregates – two-color DLA [18].

We would like to thank A. Kleczkowski and C.A. Gilligan for the helpful discussion and literature advice. E.B. Postnikov acknowledges DAAD for financial support during his stay at the Humboldt University. Partial financial support by DFG through SFB555 is gratefully acknowledged.

References

1. J.D. Murray, *Mathematical Biology I & II* (Springer, 2003)
2. W.O. Kermack, A.G. McKendrick, Proc. R. Soc. Lond. A **115**, 700 (1927)
3. R.A. Fisher, Ann. Eugenics **7**, 355 (1937)
4. A. Kolmogorov, I. Petrovsky, N. Piskounov, Moscou Univ. Bull. Math. A **1**, 1 (1937)
5. P. Haggett, *The Geographycal Structure of Epidemics* (Oxford University Press, 2000)
6. D.G. Kendall, *Mathematics and Computer Science in Biology and Medicine* (M.R.C., H.M.S.O., 1965), pp. 213−225
7. D. Mollison, J. R. Stat. Soc. B **39**, 283 (1977)
8. J. Medlock, M. Kot, Math. Biosci. **184**, 201 (2003)
9. E.B. Postnikov, I.M. Sokolov, Math. Biosciences **208**, 205 (2007)
10. P. Grassberger, Math. Biosciences **63**, 157 (1982)
11. L.M. Sander, C.P. Warren, I.M. Sokolov, C. Simon, J. Koopman, Math. Biosci. **180**, 293 (2002)
12. J. Mai, I.M. Sokolov, A. Blumen, Europhys. Lett. **44**, 7 (1998)
13. C.P. Warren, G. Mikus, E. Somfai, L.M. Sander, Phys. Rev. E **63**, 056103 (2001)
14. E. Moro, Phys. Rev. Lett. **87**, 238303 (2001)
15. C.R. Doering, C. Mueller, P. Smereka, Physica A **325**, 243 (2003)
16. E. Brunet, B. Derrida, Phys. Rev. E **56**, 2597 (1997)
17. T. Halpin-Healy, Yi-Cheng Zhang, Phys. Rep. **254**, 215 (1995)
18. E.B. Postnikov, A.B. Ryabov, A. Loskutov, J. Phys. A: Math. Theor. **40**, 12033 (2007)